

**Electronic energy gap closure and metal-insulator transition in dense liquid hydrogen**Vitaly Gorelov<sup>1</sup>, David M. Ceperley<sup>2</sup>, Markus Holzmann<sup>3,4</sup> and Carlo Pierleoni<sup>1,5</sup><sup>1</sup>*Maison de la Simulation, CEA, CNRS, Université Paris-Sud, UVSQ, Université Paris-Saclay, F-91191 Gif-sur-Yvette, France*<sup>2</sup>*Department of Physics, University of Illinois at Urbana-Champaign, Urbana, Illinois 61801, USA*<sup>3</sup>*Univ. Grenoble Alpes, CNRS, LPMMC, F-3800 Grenoble, France*<sup>4</sup>*Institut Laue Langevin, Boîte Postale 156, F-38042 Grenoble Cedex 9, France*<sup>5</sup>*Department of Physical and Chemical Sciences, University of L'Aquila, Via Vetoio 10, I-67010 L'Aquila, Italy*

(Received 3 September 2020; revised 27 October 2020; accepted 29 October 2020; published 19 November 2020)

Using quantum Monte Carlo (QMC) calculations, we investigate the insulator-metal transition observed in liquid hydrogen at high pressure. Below the critical temperature of the transition from the molecular to the atomic liquid, the fundamental electronic gap closure occurs abruptly, with a small discontinuity reflecting the weak first-order transition in the thermodynamic equation of state. Above the critical temperature, molecular dissociation sets in while the gap is still open. When the gap closes, the decay of the off-diagonal reduced density matrix shows that the liquid enters a gapless, but localized, phase: there is a crossover between the insulating and the metallic liquids. Compared to different density functional theory (DFT) functionals, our QMC calculations provide larger values for the fundamental gap and the electronic density of states close to the band edges, indicating that optical properties from DFT potentially benefit from error cancellations.

DOI: [10.1103/PhysRevB.102.195133](https://doi.org/10.1103/PhysRevB.102.195133)**I. INTRODUCTION**

The insulator-metal (IM) transition in liquid hydrogen has been an outstanding issue in high-pressure physics. Initially, the first-order transition from an insulating molecular to a metallic monoatomic fluid, called the plasma-phase transition, was predicted theoretically to occur below a critical temperature based on chemical models [1–4]. Experimentally high  $P$ - $T$  conditions necessary to observe what is now called the liquid-liquid phase transition (LLPT) can be achieved in two ways: using dynamic or static compression. Dynamically, hydrogen can be compressed with shock waves; following the time-varying changes in pressure, the metallic states can be detected via electrical, optical, and density measurements [5–13]. Metallic liquid hydrogen can also be investigated in diamond anvil cell (DAC), using controlled laser heating at a constant volume [14–19]. A rapid change in the reflectivity has been observed with both techniques, but inconsistencies between different experimental results remain.

Overall, most experiments conclude that metallization of liquid hydrogen occurs in two steps: entering first into the absorbing semiconductor regime, followed by the rapid increase in reflectivity and the IM transition. However, the behavior of the fundamental gap remains uncertain: whether there is a Mott-like temperature-activated transition accompanied by a continuous band overlap or gap closure is discontinuous and coincides with the LLPT. Here we investigate this question using quantum Monte Carlo (QMC) calculations of the fundamental gap in the vicinity of the transition.

Experimentally, the most direct information on the IM transition can be achieved via the conductivity measurements. The first experimental work that directly determined

conductivity using resistance measurements in liquid hydrogen was carried out with shock wave compression in a gas-gun experiment [5–7]. To achieve high pressures, the initial shock was split into multiple, relatively weak shocks reverberating in hydrogen between two sapphire anvils. The resistance was measured using electrodes at the hydrogen/anvil interface. Based on a (somewhat arbitrary) minimum metallic conductivity value of  $2000 (\Omega \text{ cm})^{-1}$ , the IM transition was placed at 140 GPa and 2600 K, although temperature was inferred from a model equation of state. To determine the energy gap the authors fit the conductivity in the range 93–120 GPa with a model appropriate for a liquid semiconductor with the thermally activated conductivity that depends on the mobility gap and the limiting value of conductivity.

Shock compression can as well be a laser-driven process [8,13]. The setup is almost identical to the one in a gas-gun experiment, except that the shock wave is created by laser irradiation of the pusher (Al, Be, or Cu), which is transmitted to the liquid hydrogen or deuterium. The IM transition in liquid deuterium is predicted to be first order with the critical temperature in the range  $1100 \text{ K} < T_C < 3000 \text{ K}$  and a critical pressure of about 200 GPa [13]. Based on optical measurements, two transition boundaries have been identified: first, the sample becomes opaque, corresponding to the onset of absorption at energies of the detecting laser  $\sim 2 \text{ eV}$ ; then the reflectivity increases by 30%, which is attributed to the IM transition. The band gap was estimated using empirical relations for the refractive index of semiconductors.

In a similar experiment a shock wave in deuterium was created using an electromagnetic current pulse [12]. Absorption appeared in the same  $P$ - $T$  range as in Cellier *et al.*'s experiment [13]. In this setup the reflectivity decrease upon pressure

release was monitored, and an abrupt jump was observed between 280 and 305 GPa. The temperature range (inferred from a theoretical equation of state) was between 1000 and 1800 K. The band gap was not measured directly but, based on the energy of absorption onset ( $\sim 2.3$  eV), was qualitatively compared to the reanalyzed data of Weir *et al.* [6] and to first-principles density functional theory (DFT) predictions.

Hydrogen is a very diffusive material; therefore, during static compression, it is difficult to achieve the high temperatures required to observe the IM transition. However, using short-pulse laser heating, it was possible to reach up to 3000 K in a DAC with compressed liquid hydrogen [14–17,20]. By increasing the laser power, a plateau in temperature between 1100 and 2200 K and 90 and 160 GPa [14,15,21] accompanied by the increase of reflectivity and decrease in optical transmission [16] was interpreted as being due to the latent heat, a signature of the first-order phase transition. However, a finite-element analysis (FEA) of the pulsed-laser-heated DAC predicts the latent heat necessary to reach the plateau is rather large ( $\sim 2$  eV/atom), in contrast to the theoretical predictions at the LLPT ( $\sim 0.035$  eV) [22]. The plateaus were alternatively interpreted by other authors as the onset of hydrogen absorption [12,13,23]. Measured reflectivity reached saturation at higher temperatures than the plateau [17].

Using long-pulse laser heating, another experimental group observed a similar two-stage transition: an anomalous temperature behavior and the onset of absorption followed by the rapid increase of the reflectivity [18,19]. However, the  $P$ - $T$  conditions ascribed to this transition are in disagreement with the previous DAC experiments [14–17,20]. The authors used Tauc's relation [24] to describe the observed absorption profile  $\alpha(\omega)$  of the semiconducting liquid hydrogen:  $\alpha(\omega) \propto (\hbar\omega - E_g)^2/\hbar\omega$ , where  $E_g$  is the inferred band gap.

To model the IM transition in liquid hydrogen several theoretical studies were carried out [12,22,25–33] based on Born-Oppenheimer molecular dynamics (BOMD) and path integral molecular dynamics (PIMD). The exchange-correlation (XC) approximation within DFT strongly influences the pressure and temperature of the transition [29,32–36]. More reliable QMC-based methods (coupled electron-ion Monte Carlo (CEIMC) and QMC-based molecular dynamics [25,26]) predict a transition line that is in agreement with the experimental observation of the reflective sample in most of the experiments except the one by Knudson *et al.* [34]. From BOMD and CEIMC methods the critical point terminating the transition line is expected to occur between 2000 and 3000 K at a pressure below  $\sim 150$  GPa [22,25,37]. A precise location of the critical point requires more extensive studies and gets intrinsically difficult in its close vicinity due to finite-size effects.

The electronic properties necessary to identify the IM transition, such as optical conductivity, reflectivity, and absorption, can be computed within DFT [22,25,27,28,32,33,38] by the Kubo-Greenwood formula [39,40]. Based on the HSE density functional [41] and nuclear trajectory from CEIMC [38], the DC conductivity and reflectivity jump coincides with the dissociation transition below the critical temperature, which together with the onset of absorption agrees with most experiments [13,18,20]. However, changing the XC approximation in the nuclear sampling and/or in the optical calculation gives rather different results for optical properties

and shifts the IM transition line [32,33]. Therefore, considering a correlated many-body theory, such as QMC, can give an accurate prediction of optical properties and might further serve as a benchmark for single-electron theories.

In the past, using the QMC method and the many-body Kubo formula [39,42], the electrical conductivity was computed for liquid hydrogen at temperatures above the critical point and found good agreement with the experimental results available at the time [6,7]. However, to address the IM transition it is necessary to have calculations for temperatures below and above the critical point of the LLPT. In this paper, we perform a fully consistent characterization of the IM transition in liquid hydrogen, extending to liquids our recently developed method for accurately computing energy gaps within QMC for ideal [43] and thermal crystals [44].

The very existence of a first-order liquid-liquid transition in hydrogen was questioned in a recent study based on machine learning of the DFT-PBE [54] potential observing huge finite-size effects even far away from the critical point [45]. However, these conclusions are not supported by a direct BOMD study based on DFT-PBE, where a first-order transition of similarly large systems has been reported [46].

This paper is organized as follow. Section II describes the methods used in the present study, and Sec. III reports our results on the closure of the fundamental gap of liquid hydrogen together with the benchmark of several DFT XC functionals and the discussion of optical properties. Section IV contains our conclusions.

## II. THEORETICAL METHOD

Here we report the results of an extensive study of the band gap closure of hydrogen near the LLPT using a recently developed QMC-based method [43,44]. We have studied liquid hydrogen along three isotherms:  $T = 900, 1500,$  and  $3000$  K. Nuclear quantum effects were addressed using imaginary-time path integrals for the protons. All systems considered had  $N_p = 54$  protons at constant volume and periodic boundary conditions. Optimized Slater-Jastrow-backflow trial wave functions for the electrons with twist-averaged boundary conditions have been used for the CEIMC calculations; details of the CEIMC simulations were reported in Ref. [25]. Averages over ionic positions for band gaps were obtained using at least 16 statistically independent nuclear configurations from the CEIMC trajectories.

For a given nuclear configuration we perform several reptation quantum Monte Carlo (RQMC) calculations with a varying number of electrons,  $N_e = N_p + N$ , with  $N \in [-6, 6]$  using grand canonical twist averaging (RQMC-GCTABC). We use an imaginary-time projection  $t = 2.0$  Ha $^{-1}$  and time step  $\tau = 0.01$  Ha $^{-1}$  and a  $6 \times 6 \times 6$  Monkhorst-Pack grid of twists. Electronic size effects on the gap are treated as discussed in [43]. In the grand-canonical ensemble the fundamental gap is defined as the difference in chemical potentials between adding and removing electrons,  $\mu_+$  and  $\mu_-$ , respectively (see the Supplemental Material of Ref. [44] for more details),

$$\Delta_{gc} = \mu_+ - \mu_- \simeq \left. \frac{d\langle e \rangle_{N_p}}{dn_e} \right|_{N_p^+} - \left. \frac{d\langle e \rangle_{N_p}}{dn_e} \right|_{N_p^-}, \quad (1)$$

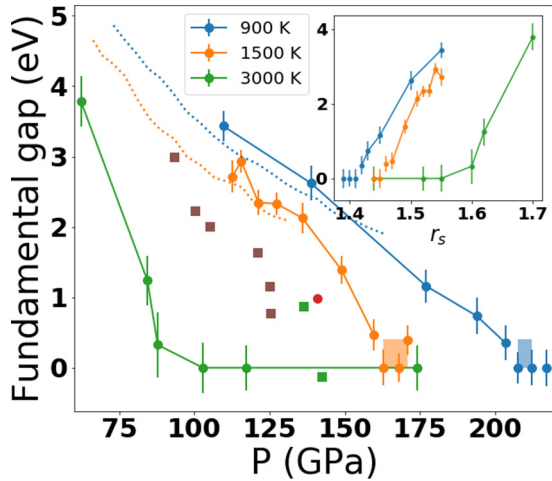


FIG. 1. The fundamental energy gap of liquid hydrogen along the isotherms:  $T = 900, 1500,$  and  $3000$  K as a function of pressure. Inset: the same gap as a function of  $r_s$ , a measure of density. The lines connect the gap data only up to the molecular-atomic transition region. The colored rectangles show the coexistence region of the LLPT according to Ref. [49]. The dotted lines are the gaps reported by Cellier *et al.* [13]. The brown and green squares are the results of Nellis *et al.* for temperatures of 2000–3000 K [7] reanalyzed in Ref. [34]. The red circle is the gap reported by McWilliams *et al.* at 2400 K [18].

where  $e$  is the energy density, expressed as a function of electronic density  $n_e = N_e/V$ ,  $\langle \dots \rangle_{N_p}$  denotes the average over the Born-Oppenheimer energy surface of the undoped  $N_e = N_p$  system, and the discontinuity in the derivative is computed at the equilibrium density  $n_e = n_p = N_p/V$ .

Optical properties were calculated within single-electron theory using the linear response Kubo-Greenwood formula [39,40]. Thermodynamic averages of optical properties were computed with the HSE XC and Williams-Lax [47,48] semiclassical approximations using at least 16 uncorrelated configurations from the CEIMC run. More details on these calculations of optical properties are given in Ref. [38]. To achieve better convergence of the DFT gaps we reanalyzed some of the HSE-DFT calculations reported in Ref. [38] with an increased  $k$ -point grid ( $8 \times 8 \times 8$ ).

To correct the band gap error when computing the optical properties within DFT, one can rigidly shift the unoccupied eigenvalues by the QMC-DFT gap difference,  $\Delta_{sc} = \Delta_{QMC} - \Delta_{DFT}$ . This defines the “scissor” correction. Alternatively, it is possible to shift the obtained Kubo-Greenwood conductivity directly by  $\Delta_{sc}$ . We verified that the two procedures are, in fact, equivalent.

### III. RESULTS

#### A. The fundamental gap

Figure 1 shows the estimates of the fundamental gap, computed according to Eq. (1), for different isotherms of liquid hydrogen. The gap gradually decreases with pressure and depends on both temperature and density, as can be seen in the inset. Below the critical temperature of the LLPT, the gap closure coincides with the beginning of the coexistence region,

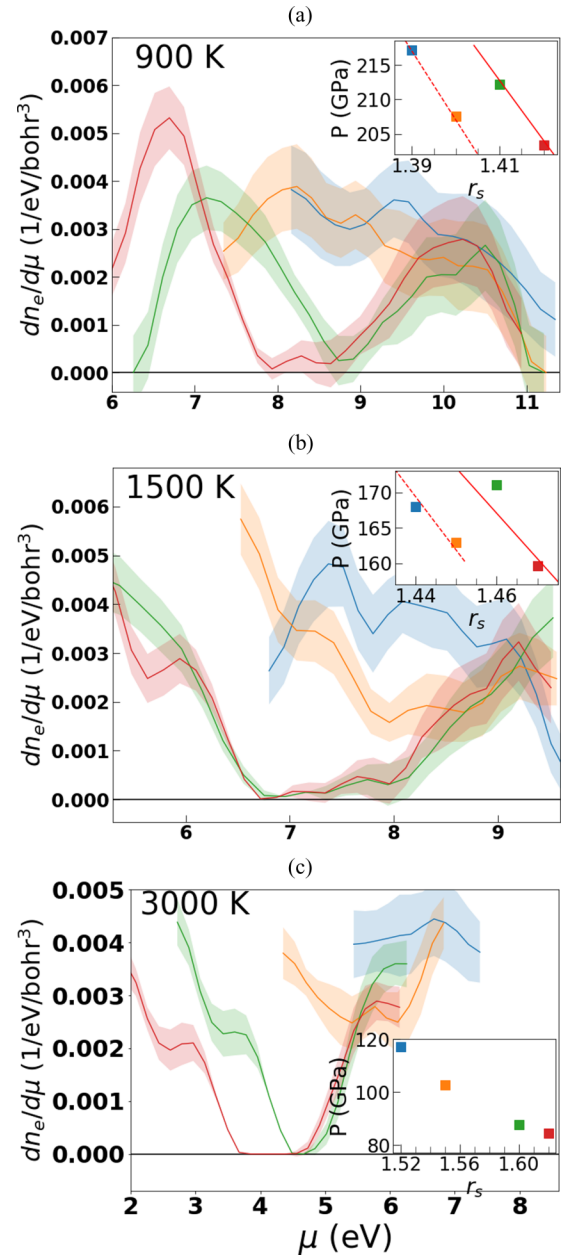


FIG. 2. Density of states of liquid hydrogen near the band edge at densities near the gap closure for three isotherms: (a) 900 K, (b) 1500 K, and (c) 3000 K. The insets show the equation of state as reported in [49]. The dashed and solid red lines indicate the atomic and molecular regions, respectively. The colors of the DOS match the colors of points in the insets.

as indicated by colored rectangles. In this region the accuracy of the estimated gap is uncertain since during the simulation at constant volume the system dynamically switches from atomic to molecular states and back. Note that at all temperatures the gap decreases linearly with pressure, with the slope becoming steeper as temperature increases.

From the electronic density of states (DOS), shown in Fig. 2, we obtain important information on the character of the transition. Below the critical temperature, at 1500 and 900 K, we show the DOS at four densities around the LLPT.

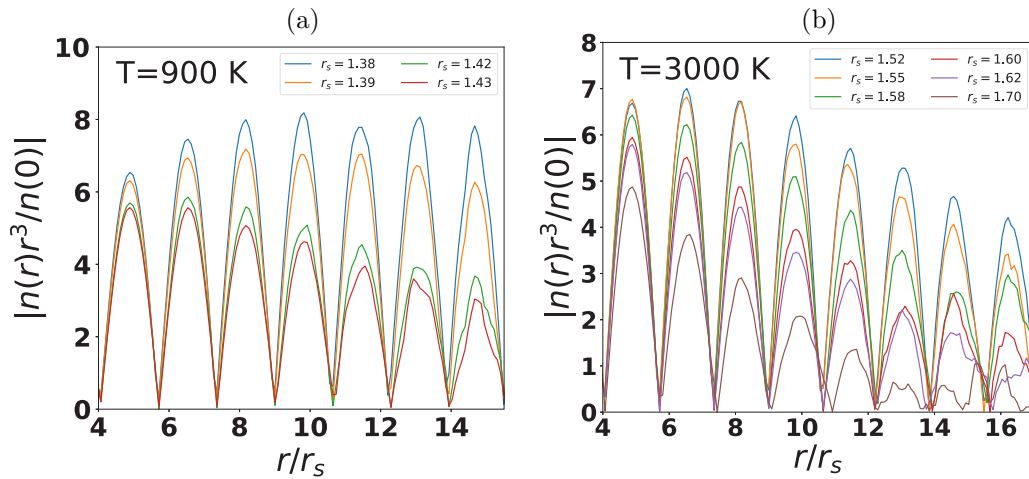


FIG. 3. The absolute value of the off-diagonal part of the reduced single-particle density matrix,  $n(r)$  [51], multiplied by  $r^3$  as a function of distance  $r$  for various densities around the gap closure. (a) At  $T = 900$  K, when the gap vanishes for  $r_s \lesssim 1.42$ , as the liquid crosses the LLPT,  $n(r)$  changes, indicating more delocalized, Fermi-liquid-like behavior. (b) At  $T = 3000$  K, since  $n(r)$  decays faster than  $r^{-3}$  at all densities, the electron liquid remains localized even when the gap vanishes ( $r_s \lesssim 1.55$ ).

The equation of state is plotted in the inset as reported in Ref. [49]. On the molecular side (higher  $r_s$ ), the DOS has a clearly visible gap where the density of states is almost vanishing. Although the finite system size and the finite number of nuclear configurations underlying our calculations do not allow us to distinguish between a strictly vanishing DOS in the thermodynamic limit and a semiconductor DOS containing a small fraction of disorderlike (impurity) states inside the gap, the shape of the DOS changes abruptly from the molecular to the atomic liquid. The width of the gap continuously follows the molecular branch inside the coexistence region, strongly supporting a scenario where the gap vanishes discontinuously at the molecular-atomic transition.

Above the critical temperature, at 3000 K, the DOS reflects the mixed molecular-atomic character of the liquid. Although more calculations between  $r_s = 1.6$  (green point), where the gap is 0.8 eV, and  $r_s = 1.55$  (orange point), where the gap is closed, are needed to precisely locate the closure of the gap, the strong correlation of the DOS with the molecular character suggests that the gap closes continuously as a function of density (see the inset of Fig. 1) and thus also as a function of pressure.

The molecular fraction as a function of pressure was analyzed in Ref. [49] based on different criteria. Although all estimators used in that reference show the onset of molecular dissociation within the gapped liquid, the values of the molecular fraction are sensitive to the estimator. This implies that we cannot determine whether a gapped atomic liquid is reached before gap closure.

In a normal solid, the vanishing of the gap usually implies an IM transition, e.g., a transition from a state of almost vanishing conductivity to a state where electronic conductivity is limited by only nuclear (phononic) motion and/or impurities. However, a liquid is similar to a disordered system; the vanishing of the gap does not necessarily imply the existence of extended states at the Fermi level needed for electronic transport. Further information on the extended/localized character of the states around the Fermi level is needed in

order to determine the insulating or metallic character of the liquid [50].

The QMC results for electronic momentum distribution and its Fourier transform, the reduced single-particle density matrix along the LLPT, were presented and analyzed in Ref. [51]. The asymptotic behavior of the off-diagonal part of the single-electron density matrix  $n(r)$  at large distances  $r$  discriminates between extended and localized states, the latter decaying faster than  $r^{-3}$  [25]. Below the critical temperature, the off-diagonal part of the density matrix abruptly changes from a roughly exponential decay in the molecular phase to an algebraic Fermi-liquid-like behavior in the atomic liquid. As seen in Fig. 3(a), at  $T = 900$  K, for densities below the transition ( $r_s = 1.42$  and  $1.43$ ) the envelope of  $n(r)$  decays faster than  $r^{-3}$ , whereas in the atomic gapless region ( $r_s = 1.38$  and  $r_s = 1.39$ ) the envelope of  $n(r)r^3$  remains approximately constant at large distances, indicating extended states. Therefore, the closure of the gap induces an IM transition which occurs together with the thermodynamic molecular-atomic transition.

Above the critical point the situation is different; the momentum distribution changes smoothly with density, as seen in Fig. 3(b). We see that the envelope of  $n(r)$  decays faster than  $r^{-3}$  at  $T = 3000$  K for the densities below and above gap closure, implying a localized electron liquid. At gap closure, the liquid enters a gapless localized phase. This enables absorption at arbitrary low energies. We expect no sharp IM transition but a crossover to the metallic liquid since electronic delocalization increases smoothly with density or pressure. Indeed, conductivity and other transport properties obtained within DFT change smoothly above the critical temperature [22,31,38]. We further note that the DOS after gap closure shown in Fig. 2 actually resembles that of a dirty semiconductor containing localized (disordered) states inside the gap.

We now compare our results to experimental estimates [7,13,18]. Cellier *et al.* [13] extracted the gap values, reported as dotted lines in our Fig. 1, based on the empirical relations to the refractive index data (as discussed in detail in the Supplemental Material of Ref. [13]). The agreement with our

results is rather good, although the experiment is for deuterium. However, our result does not support the extrapolation procedure provided in the paper. Another estimate of the gap is based on the semiconductor model of thermally activated conductivity [7]

$$\sigma(\rho, T) = \sigma_0 \exp[-E_g(\rho)/2k_B T], \quad (2)$$

where  $\sigma_0$  is the limiting value of conductivity and  $E_g(\rho)$  is the energy gap, assumed to depend linearly on the density  $\rho$  and be independent of temperature  $T$ . Note that in the original paper of Nellis *et al.* [7] the choice of the limiting value of conductivity  $\sigma_0$  was arbitrary;  $\sigma_0$  is a free parameter that varied between 66 and 300  $(\Omega \text{ cm})^{-1}$ , a value typical of liquid semiconductors [52]. In Fig. 1 we report results of Nellis *et al.* [7] reanalyzed by Knudson *et al.* [34], who used a different equation of state [53] and different values of  $\sigma_0$ . They assumed that hydrogen before the transition behaves like a fluid semiconductor, where the conductivity is progressively increased upon the closure of the gap with density. The value of  $\sigma_0$  was chosen so the resulting gap was not negative. The gap is assumed to weakly depend on temperature, which was not measured and, according to the latest equation of state [53], varied between 2000 and 3000 K, increasing towards the higher pressure [34]. Below the critical temperature, our results do not fully support this model, as the QMC density of states increases rapidly at the transition (see Fig. 2), and our gap is temperature dependent. Above the critical temperature, we do not have enough data to assess the model, as we would need at least three isotherms, but the form of the DOS discussed above supports the use of a semiconductor model.

Last, analyzing the absorption profile with the Tauc model [24], McWilliams *et al.* [18] reported a gap value of 0.9 eV at 2400 K and 140 GPa [18]. To assess the validity of this model, we analyzed several theoretical absorption profiles with DFT-HSE for two densities ( $r_s = 1.54$  and 1.47) at  $T = 1500$  K. We found that the fitting of the theoretical absorption to the Tauc model slightly overestimates the values of the gaps (by  $\sim 0.3$  eV), computed at the same level of approximation as the optical properties, e.g., DFT-HSE. This is shown in Fig. 4. However, the Tauc model gives good agreement with the QMC gap, indicating the possibility of error cancellation, when calculating the spectra.

### B. Benchmark of XC approximations

Figure 5(a) shows the value of the gap using different DFT functionals compared to the thermal gap from RQMC-GCTABC at 1500 K and  $r_s = 1.54$ . Five functionals were considered: the generalized gradient approximation (GGA) with the PBE [54] functional, nonlocal and semilocal van der Waals density functionals (rVV10 [55] and vdW-DF2 [56]), the semilocal meta-GGA TPSS functional [57], and nonlocal hybrid HSE [41]. The differences are on the order of  $\sim 1$ -2 eV, with HSE and vdW-DF2 being the closest to the QMC prediction, a result similar to that for solid hydrogen [44]. We also access the accuracy of the intensity of optical properties computed with different XC functionals. With QMC we do not have direct access to the optical properties, but to a large extent they are defined by the density of states. In Fig. 5(b) we show for each DFT approximation the difference of the inte-

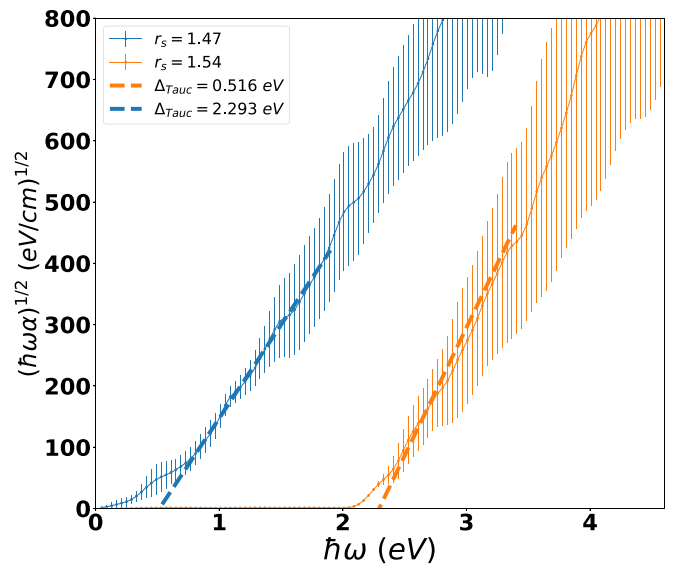


FIG. 4. Tauc analysis of the absorption profiles, computed with DFT-HSE for liquid hydrogen at  $T = 1500$  K and two densities:  $r_s = 1.54$  and 1.47.

grated density of states between QMC and gap-corrected DFT DOS (we correct the value of the gap to match the QMC one). As with the gap comparison, HSE and vdW-DF2 perform better than the others. Note that the vdW-DF2 performs better on the conduction side, and HSE is better on the valence side. Therefore, considering the computational cost of nonlocal hybrid functionals, it might be advantageous to use semilocal vdW-DF2. Another important conclusion from Fig. 5 is that correcting just the gap error in DFT does not guarantee that the intensities of the spectra are accurate; they are probably underestimated within the XC approximations since the difference between the QMC and DFT DOS is always positive, implying that there are fewer states contributing to the DFT spectrum.

In Ref. [33], the liquid-liquid transition was studied using PIMD with the rVV10 functional providing highest occupied molecular orbital (HOMO) and lowest unoccupied molecular orbital (LUMO) band gaps computed within the SCAN-L functional [58]. In the common density and temperature regions, the reported HOMO-LUMO gaps are roughly comparable to the QMC values. However, the procedure of Ref. [33] of assigning the HOMO-LUMO gaps in the liquid essentially relies on the underlying single-particle theory and differs from the calculation of the fundamental gap discussed here. Moreover, the sampling of nuclear trajectories in the present work and in Ref. [33] are different; this significantly influences the value of the computed gap, making a quantitative comparison impractical.

### C. Optical properties

In Fig. 6(a) we compare HSE and QMC gaps versus pressure along the three isotherms. We notice a constant shift of roughly  $\sim 1$  eV between HSE and QMC gaps below the critical temperature. At the highest temperature,  $T = 3000$  K above the critical point, the difference decreases with increasing pressure. The gap closes at the same values of pressure

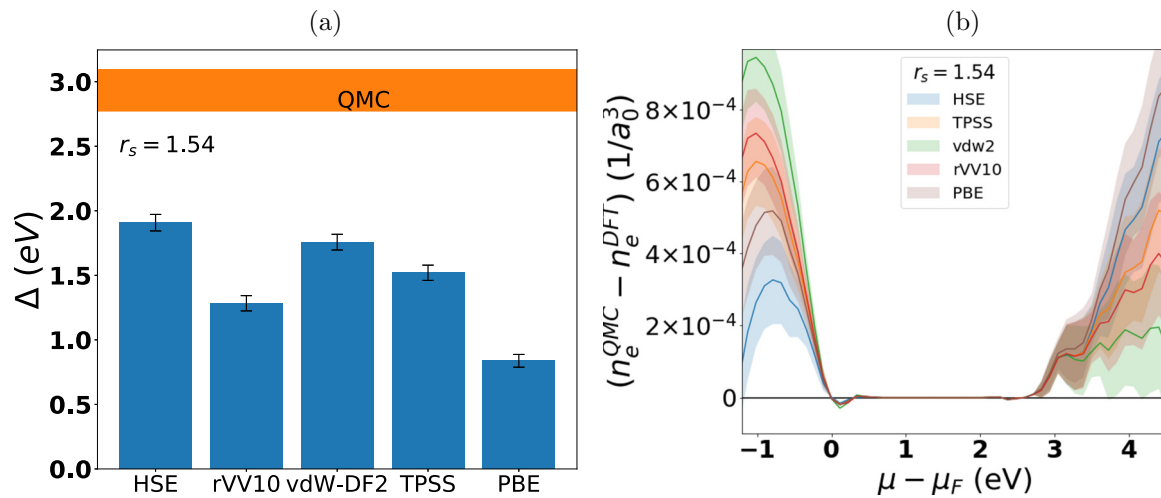


FIG. 5. (a) The fundamental gap calculated with different DFT exchange correlation functionals compared with the QMC gap at  $T = 1500$  K and  $r_s = 1.54$ . The orange horizontal bar is the RQMC-GCTABC thermal gap with its statistical uncertainty given by its width. (b) Difference between the integrated density of states of QMC and DFT. A “scissor correction” on the horizontal axis from the gap value was applied to the DFT profiles before subtracting them from the QMC profile;  $\mu_F$  has been set by the maximum of the valence band.

with DFT and QMC at 3000 and 15 000 K, while at  $T = 900$  K the HSE gap closes at 180 GPa, while the QMC gap closes at  $\sim 200$  GPa. Figure 6(b) shows that when shifting the HSE eigenvalues to match the QMC gap, the value of absorption at 2.3 eV, plotted as a function of pressure, decreases, with the shift being more pronounced at lower pressures and lower temperatures. At high pressure, when the gap is already closed, we cannot apply the scissor correction, and the value of absorption at 2.3 eV will be based purely on the optical transition intensity, which we cannot currently calculate within QMC. The DOS in Fig. 5(b) suggests that the DFT optical intensities might be underestimated, as the QMC DOS is higher near the gap; therefore, we expect an error cancellation between an underestimated band gap and underestimated intensities to occur. This error cancellation would explain the good agreement of DFT-HSE predictions with experiments previously observed [38]

The reflectivity can be reanalyzed in the same manner. Consistent with decreased absorption at lower pressure, reflectivity decreases as well. However, we do not provide the same analyses here for the following reason: we are interested in the IM transition, which is characterized by typical values of reflectivity of  $\sim 0.3$ ; the gap at this value is either small or already closed, and the correction will be negligible. The pressure at which reflectivity reaches 0.3, according to [38], is reported in Fig. 6(a) as colored squares. Therefore, correcting the gap for the reflectivity will not produce significant changes; the accuracy of optical properties will be determined by the accuracy of the intensities of optical transitions.

The pressure at which hydrogen turns opaque was attributed in several experiments to correspond to the absorption of  $\sim 1 \mu\text{m}^{-1}$  [12,13,18]. Based on our QMC-shifted HSE absorption, we predict that the onset of absorption will shift to higher pressures, with respect to the previously reported

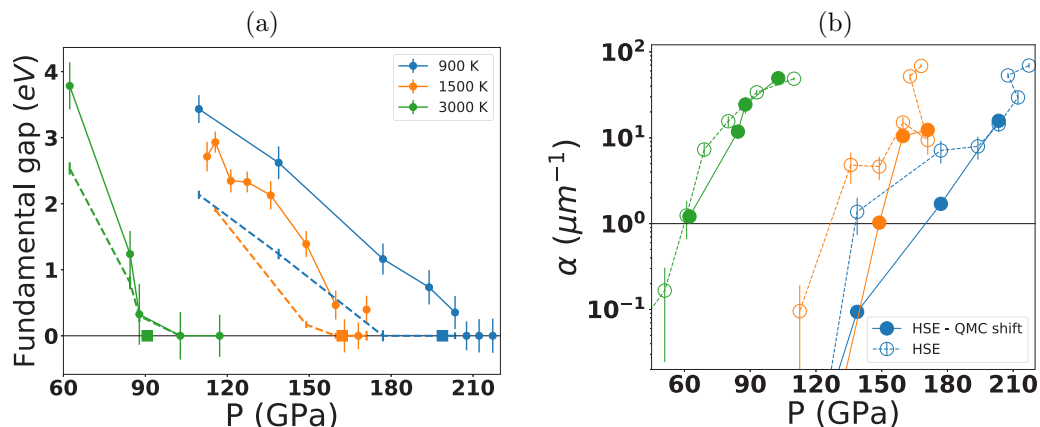


FIG. 6. (a) The HSE and QMC band gaps along three isotherms. The dashed lines are the HSE values, and solid lines are the QMC results. Squares indicate pressures at which the reflectivity is 0.3 according to Ref. [38]. (b) Absorption at  $\omega = 2.3$  eV along the  $T = 1500$  K isotherm. The dashed lines are the HSE values reported in Ref. [38], and the solid lines are computed using the QMC-corrected band gaps.

ones [38]. This again indicates that the absorption intensities might be underestimated within the HSE XC approximation.

#### IV. CONCLUSION

In this paper, we have reported values of the fundamental gap across the pressure-induced molecular dissociation region in hydrogen extending the QMC method developed in Ref. [43]. The main finding is that gap closure strongly correlates with the beginning of the molecular dissociation transition. Below the critical temperature, the gap closure occurs abruptly, with a small discontinuity reflecting the weak first-order thermodynamic transition. Above the critical temperature, molecular dissociation begins before the closing of the gap. Despite the liquid becoming gapless, the change from insulating to metallic behavior occurs progressively. On the basis of our QMC density of states, we have further benchmarked different DFT functionals and found that all considered functionals underestimate the gap. After applying a scissor correction to the energy spectrum, HSE XC optical transition intensities, previously found to agree with experiments [38], are now lower and in less good agreement with experiments [see

Fig. 6(b)]. Our analysis of the DOS at the band edges [see Fig. 5(b)] suggests that the QMC spectrum has more states than DFT ones and hence should have larger intensity, possibly restoring the agreement with experiments. In other words, our analysis suggests that the previously observed agreement between HSE optical profiles and experiments [38] profited by error cancellation. This observation remains to be established by a more systematic investigation.

#### ACKNOWLEDGMENTS

D.M.C. was supported by DOE Grant No. NA DE-NA0001789 and by the Fondation NanoSciences (Grenoble). V.G. and C.P. were supported by the Agence Nationale de la Recherche (ANR) France, under the program “Accueil de Chercheurs de Haut Niveau 2015,” project HyLightExtreme. Computer time was provided by PRACE Project No. 2016143296, ISCRAB (IsB17\_MMCRHY) computer allocation at CINECA Italy, the high-performance computer resources from Grand Equipement National de Calcul Intensif (GENCI) Allocation No. 2018-A0030910282, and the Froggy platform of CIMENT, Grenoble (Rhône-Alpes CPER07-13 CIRA and ANR-10-EQPX-29-01).

- 
- [1] L. Landau and Y. B. Zeldovich, *Acta Physicochim. USSR* **18**, 194 (1943).
- [2] G. É. Norman and A. N. Starostin, *J. Appl. Spectrosc.* **13**, 965 (1970).
- [3] W. Ebeling and W. Richert, *Phys. Lett. A* **108**, 80 (1985).
- [4] D. Saumon and G. Chabrier, *Phys. Rev. Lett.* **62**, 2397 (1989).
- [5] W. J. Nellis, A. C. Mitchell, P. C. McCandless, D. J. Erskine, and S. T. Weir, *Phys. Rev. Lett.* **68**, 2937 (1992).
- [6] S. T. Weir, A. C. Mitchell, and W. J. Nellis, *Phys. Rev. Lett.* **76**, 1860 (1996).
- [7] W. J. Nellis, S. T. Weir, and A. C. Mitchell, *Phys. Rev. B* **59**, 3434 (1999).
- [8] P. M. Celliers, G. W. Collins, L. B. Da Silva, D. M. Gold, R. Cauble, R. J. Wallace, M. E. Foord, and B. A. Hammel, *Phys. Rev. Lett.* **84**, 5564 (2000).
- [9] P. Loubeyre, P. M. Celliers, D. G. Hicks, E. Henry, A. Dewaele, J. Pasley, J. Eggert, M. Koenig, F. Occelli, K. M. Lee, R. Jeanloz, D. Neely, A. Benuzzi-Mounaix, D. Bradley, M. Bastea, S. Moon, and G. W. Collins, *High Pressure Res.* **24**, 25 (2004).
- [10] P. Loubeyre, S. Brygoo, J. Eggert, P. M. Celliers, D. K. Spaulding, J. R. Rygg, T. R. Boehly, G. W. Collins, and R. Jeanloz, *Phys. Rev. B* **86**, 144115 (2012).
- [11] V. E. Fortov, R. I. Ilkaev, V. A. Arinin, V. V. Burtzev, V. A. Golubev, I. L. Iosilevskiy, V. V. Khrustalev, A. L. Mikhailov, M. A. Mochalov, V. Y. Ternovoi, and M. V. Zhernokletov, *Phys. Rev. Lett.* **99**, 185001 (2007).
- [12] M. D. Knudson, M. P. Desjarlais, A. Becker, R. W. Lemke, K. R. Cochrane, M. E. Savage, D. E. Bliss, T. R. Mattsson, and R. Redmer, *Science* **348**, 1455 (2015).
- [13] P. M. Celliers, M. Millot, S. Brygoo, R. S. McWilliams, D. E. Fratanduono, J. R. Rygg, A. F. Goncharov, P. Loubeyre, J. H. Eggert, J. L. Peterson, N. B. Meezan, S. Le Pape, G. W. Collins, R. Jeanloz, and R. J. Hemley, *Science* **361**, 677 (2018).
- [14] V. Dzyabura, M. Zaghoo, and I. F. Silvera, *Proc. Natl. Acad. Sci. USA* **110**, 8040 (2013).
- [15] K. Ohta, K. Ichimaru, M. Einaga, S. Kawaguchi, K. Shimizu, T. Matsuoka, N. Hirao, and Y. Ohishi, *Sci. Rep.* **5**, 16560 (2015).
- [16] M. Zaghoo, A. Salamat, and I. F. Silvera, *Phys. Rev. B* **93**, 155128 (2016).
- [17] M. Zaghoo and I. F. Silvera, *Proc. Natl. Acad. Sci. USA* **114**, 11873 (2017).
- [18] R. S. McWilliams, D. A. Dalton, M. F. Mahmood, and A. F. Goncharov, *Phys. Rev. Lett.* **116**, 255501 (2016).
- [19] S. Jiang, N. Holtgrewe, Z. M. Geballe, S. S. Lobanov, M. F. Mahmood, R. S. McWilliams, and A. F. Goncharov, *Adv. Sci.* **7**, 1901668 (2020).
- [20] M. Zaghoo, R. J. Husband, and I. F. Silvera, *Phys. Rev. B* **98**, 104102 (2018).
- [21] M. Zacharias and F. Giustino, *Phys. Rev. B* **94**, 075125 (2016).
- [22] M. A. Morales, C. Pierleoni, E. Schwegler, and D. M. Ceperley, *Proc. Natl. Acad. Sci. USA* **107**, 12799 (2010).
- [23] A. F. Goncharov and Z. M. Geballe, *Phys. Rev. B* **96**, 157101 (2017).
- [24] J. Tauc, *Mater. Res. Bull.* **3**, 37 (1968).
- [25] C. Pierleoni, M. A. Morales, G. Rillo, M. Holzmann, and D. M. Ceperley, *Proc. Natl. Acad. Sci. USA* **113**, 4954 (2016).
- [26] G. Mazzola, R. Helled, and S. Sorella, *Phys. Rev. Lett.* **120**, 025701 (2018).
- [27] W. Lorenzen, B. Holst, and R. Redmer, *Phys. Rev. B* **82**, 195107 (2010).
- [28] B. Holst, M. French, and R. Redmer, *Phys. Rev. B* **83**, 235120 (2011).

- [29] M. A. Morales, J. M. McMahon, C. Pierleoni, and D. M. Ceperley, *Phys. Rev. Lett.* **110**, 065702 (2013).
- [30] G. E. Norman and I. M. Saitov, *Contrib. Plasma Phys.* **58**, 122 (2018).
- [31] V. Gorelov, C. Pierleoni, and D. M. Ceperley, *Contrib. Plasma Phys.* **59**, e201800185 (2019).
- [32] B. Lu, D. Kang, D. Wang, T. Gao, and J. Dai, *Chin. Phys. Lett.* **36**, 103102 (2019).
- [33] J. Hinz, V. V. Karasiev, S. X. Hu, M. Zaghoo, D. Mejía-Rodríguez, S. B. Trickey, and L. Calderín, *Phys. Rev. Res.* **2**, 032065(R) (2020).
- [34] M. D. Knudson, M. P. Desjarlais, M. Preising, and R. Redmer, *Phys. Rev. B* **98**, 174110 (2018).
- [35] K. Ramakrishna, T. Dornheim, and J. Vorberger, *Phys. Rev. B* **101**, 195129 (2020).
- [36] H. Y. Geng, Q. Wu, M. Marqués, and G. J. Ackland, *Phys. Rev. B* **100**, 134109 (2019).
- [37] S. van de Bund, H. Wiebe, and G. J. Ackland, [arXiv:2009.05491](https://arxiv.org/abs/2009.05491).
- [38] G. Rillo, M. A. Morales, D. M. Ceperley, and C. Pierleoni, *Proc. Natl. Acad. Sci. USA* **116**, 9770 (2019).
- [39] R. Kubo, *J. Phys. Soc. Jpn.* **12**, 570 (1957).
- [40] D. A. Greenwood, *Proc. Phys. Soc.* **71**, 585 (1958).
- [41] J. Heyd, J. E. Peralta, G. E. Scuseria, and R. L. Martin, *J. Chem. Phys.* **123**, 174101 (2005).
- [42] F. Lin, M. A. Morales, K. T. Delaney, C. Pierleoni, R. M. Martin, and D. M. Ceperley, *Phys. Rev. Lett.* **103**, 256401 (2009).
- [43] Y. Yang, V. Gorelov, C. Pierleoni, D. M. Ceperley, and M. Holzmann, *Phys. Rev. B* **101**, 085115 (2020).
- [44] V. Gorelov, M. Holzmann, D. M. Ceperley, and C. Pierleoni, *Phys. Rev. Lett.* **124**, 116401 (2020).
- [45] B. Cheng, G. Mazzola, C. J. Pickard, and M. Ceriotti, *Nature (London)* **585**, 217 (2020).
- [46] T. Bryk, C. Pierleoni, G. Ruocco, and A. P. Seitsonen, *J. Mol. Liq.* **312**, 113274 (2020).
- [47] F. E. Williams, *J. Chem. Phys.* **19**, 457 (1951).
- [48] M. Lax, *J. Chem. Phys.* **20**, 1752 (1952).
- [49] C. Pierleoni, M. Holzmann, and D. M. Ceperley, *Contrib. Plasma Phys.* **58**, 99 (2018).
- [50] W. Kohn, *Phys. Rev.* **133**, A171 (1964).
- [51] C. Pierleoni, G. Rillo, D. M. Ceperley, and M. Holzmann, *J. Phys.: Conf. Ser.* **1136**, 012005 (2018).
- [52] A. Lösche, *Krist. Tech.* **7**, K55 (1972).
- [53] G. Kerley, *Sandia National Laboratories Report No. SAND2003-3613*, Sandia National Laboratories, 2003.
- [54] J. P. Perdew, K. Burke, and M. Ernzerhof, *Phys. Rev. Lett.* **78**, 1396(E) (1997).
- [55] R. Sabatini, T. Gorni, and S. de Gironcoli, *Phys. Rev. B* **87**, 041108(R) (2013).
- [56] K. Lee, É. Murray, L. Kong, B. Lundqvist, and D. Langreth, *Phys. Rev. B* **82**, 081101(R) (2010).
- [57] J. Tao, J. P. Perdew, V. N. Staroverov, and G. E. Scuseria, *Phys. Rev. Lett.* **91**, 146401 (2003).
- [58] D. Mejía-Rodríguez and S. B. Trickey, *Phys. Rev. A* **96**, 052512 (2017).